Journal of
Astronomical Telescopes,
Instruments, and Systems

AstronomicalTelescopes.SPIEDigitalLibrary.org

Multiconjugate adaptive optics simulator for the Thirty Meter Telescope: design, implementation, and results

Etsuko Mieda
Jean-Pierre Veran
Matthias Rosensteiner
Paolo Turri
David Andersen
Glen Herriot
Olivier Lardiere
Paolo Spano

SPIE.

Etsuko Mieda, Jean-Pierre Veran, Matthias Rosensteiner, Paolo Turri, David Andersen, Glen Herriot, Olivier Lardiere, Paolo Spano, "Multiconjugate adaptive optics simulator for the Thirty Meter Telescope: design, implementation, and results," *J. Astron. Telesc. Instrum. Syst.* **4**(4), 049002 (2018), doi: 10.1117/1.JATIS.4.4.049002.

Journal of Astronomical Telescopes, Instruments, and Systems 4(4), 049002 (Oct–Dec 2018)

Multiconjugate adaptive optics simulator for the Thirty Meter Telescope: design, implementation, and results

Etsuko Mieda,[a,*] Jean-Pierre Veran,[b] Matthias Rosensteiner,[c] Paolo Turri,[d] David Andersen,[b] Glen Herriot,[b] Olivier Lardiere,[b] and Paolo Spano[e]
[a]Subaru Telescope, Hilo, Hawaii, United States
[b]National Research Council Herzberg Astronomy and Astrophysics, Victoria, Canada
[c]Max Planck Institute for Extraterrestrial Physics, Garching, Germany
[d]University of California, Berkeley, California, United States
[e]Officina Stellare, Sarcedo (VI), Italy

Abstract. We present a multiconjugate adaptive optics (MCAO) system simulator bench, Herzberg NFIRAOS Optical Simulator (HeNOS). HeNOS is developed to validate the performance of the MCAO system for the Thirty Meter Telescope, as well as to demonstrate techniques critical for future AO developments. We focus on describing the derivations of parameters that scale the 30-m telescope AO system down to a bench experiment and explain how these parameters are practically implemented on an optical bench. While referring to other papers for details of AO technique developments using HeNOS, we introduce the functionality of HeNOS, in particular, three different single-conjugate AO modes that HeNOS currently offers: a laser guide star AO with a Shack–Hartmann wavefront sensor, a natural guide star AO with a pyramid wavefront sensor, and a laser guide star AO with a sodium spot elongation on the Shack–Hartmann corrected by a truth wavefront sensing on a natural guide star. Laser tomography AO and ultimate MCAO are being prepared to be implemented in the near future. [DOI: 10.1117/1.JATIS.4.4.049002]

Keywords: adaptive optics; astronomy; wavefront sensors; Thirty Meter Telescope; pyramid wavefront sensors.

Paper 18009P received Feb. 22, 2018; accepted for publication Sep. 5, 2018; published online Sep. 24, 2018.

1 Introduction

Narrow Field InfraRed Adaptive Optics System (NFIRAOS)[1] will be the first adaptive optics (AO) system to be deployed on the Thirty Meter Telescope (TMT). NFIRAOS is a multiconjugate (MC) AO system equipped with six laser guide stars (LGSs), six LGS wavefront sensors (WFSs) made with Shack–Hartmann (SH) WFSs, two deformable mirrors (DMs), and a natural guide star (NGS) truth wavefront sensor (TWFS). NFIRAOS will provide near diffraction limited correction over 10 to 30 arcsec and partial correction over 2 arcmin in near-infrared. The unprecedented scale of NFIRAOS prompts us to build the Herzberg NFIRAOS Optical Simulator (HeNOS) bench at the National Research Council Herzberg for Astronomy and Astrophysics in Canada. The main purpose of this bench is to demonstrate the robustness and performance stability of an NFIRAOS-like MCAO system in realistic and varying conditions.

In this paper, we present the design and implementation of HeNOS and describe the bench capability to introduce AO development applications. Our work is organized as follows. A derivation of the bench parameters drawn from the NFIRAOS parameters and constraints is shown in Sec. 2. The components of the bench and how they are implemented on an optical bench are described in Sec. 3. The new implementation of a TWFS made with a pyramid wavefront sensor (PWFS) can be found in Secs. 3.8 and 3.9. Section 4 describes three different AO modes that HeNOS offers today. Finally, we summarize the current bench status and discuss the future HeNOS plan in Sec. 5.

2 Bench Parameters

The challenge in designing the HeNOS bench is to scale the AO system from a 30-m telescope down to a bench size experiment. In this section, we describe how the bench parameters are derived from the NFIRAOS parameters. The parameter subscripts N and H refer to NFIRAOS and HeNOS, respectively. The earlier bench design development can be found in Ref. 2.

The first set of constraints arises from the need to keep the cost down. The first cost-related constraint is the necessity to work at visible wavelength in order to simplify optics alignment and to use inexpensive CCD or CMOS detectors, such as our PointGrey Grasshopper CCDs, for WFS and imaging. We have set $\lambda_H = 0.670\ \mu m$ as both our sensing and imaging (science) wavelength for the HeNOS bench to match the laser diode we had available as a light source.

The second cost-related constraint is the necessity to work with relatively low order (thus economical) DMs. On HeNOS, we have two Alpao magnetic DMs. DM0 is a 11×11 DM with ~ 9 actuator pitches across the clear aperture (n_H), conjugated to ground, and DM1 is 19×19 DM with $n_H \sim 16$, which is conjugated to a high altitude. Both DMs have the same physical actuator pitch of 1.5 mm. If we simulate a $D_H = 30$ m telescope with $n_H = 9$ across all NGS beams, diffraction-limited imaging could only be achieved with unrealistically weak turbulence. Diffraction-limited imaging is possible as long as the turbulence, r_0, is not significantly less than $d_H = D_H/n_H$ at λ_H. We have found that $D_H = 8$ m

---

*Address all correspondence to: Etsuko Mieda, E-mail: MIEDA@NAOJ.ORG is about the largest feasible diameter that we can scale down to a bench size with our DMs. Consequently, we have set the telescope diameter to simulate with HeNOS to $D_{\mathrm{H}} = 8$ m. It follows that the DM actuator pitch projected on this diameter is: $d_{\mathrm{H}} = D_{\mathrm{H}}/9 = 0.89$ m.

The third cost-related constraint is the necessity to limit the field of view (FOV) of the system. Considering the size of the telescope, we are trying to simulate (8 m) and the size of our DMs (13.5 mm footprint for an NGS beam); in any case, given the desire to work with off-the-shelf optical elements in an affordable size (i.e., 1 to 2 in.), we have found, after several iterations of the optical design, that the FOV had to be limited to $\mathrm{FOV_H} = 10.9$ arcsec on the sky. This is significantly smaller than the NFIRAOS FOV, which is $\mathrm{FOV_N} = 120$ arcsec on the sky. Note that this constraint was not integrated in the derivations from Ref. 2.

Within the above set of constraints, we now set three objectives to guide our bench design:

- Objective 1: HeNOS should have the ability to achieve diffraction limited imaging on axis. This constrains the simulated turbulence to have $r_{0,\mathrm{H}}(\lambda_H) \sim d_{\mathrm{H}} = 0.89$ m.
- Objective 2: After MCAO correction, HeNOS and NFIRAOS should have the same point spread function (PSF) uniformity across their respective FOV. This is achieved if the ratio θ_2/FOV is the same for HeNOS as for NFIRAOS, where θ_2 is the generalized anisoplanatism angle after two DM corrections. This objective guarantees that the corrected field of HeNOS and NFIRAOS will look alike.
- Objective 3: HeNOS and NFIRAOS should have the same θ_0/FOV ratio. This makes it just as hard for HeNOS and NFIRAOS to achieve Objective 2.

These objectives ensure that HeNOS has similar wide-field performance as NFIRAOS under similarly difficult turbulence conditions. These similarities ensure that the model used to predict the NFIRAOS performance will work under similar conditions as when it is used in the HeNOS configuration that is supposed to demonstrate its validity as discussed in the introduction. The similarities also ensure that the algorithms under tests (such as truth sensing, LGS-NGS tomography, and PSF reconstruction) will be validated conditions similar to that in which they are expected to be used in NFIRAOS.

In order to achieve our three objectives, we start with $r_{0,\mathrm{H}}(\lambda_H) = 0.89$ m. The isoplanatic angle is obtained as $\theta_0 = 0.3147 r_0/h_0$ where h_0 is the weighted average altitude of the turbulence. For the NFIRAOS median profile given in Table 1, $h_{0,\mathrm{N}} \sim 5.2$ km. Objective 3 can be written as

$$\frac{\theta_{0,\mathrm{H}}(\lambda_{\mathrm{H}})}{\theta_{0,\mathrm{N}}(\lambda_{\mathrm{H}})} = \frac{r_{0,\mathrm{H}}(\lambda_{\mathrm{H}})}{r_{0,\mathrm{N}}(\lambda_{\mathrm{H}})} \frac{h_{,0,\mathrm{N}}}{h_{0,\mathrm{H}}} = \frac{\mathrm{FOV_H}}{\mathrm{FOV_N}}. \tag{1}$$

With $\mathrm{FOV_H}$ constrained to 10.9 arcsec, the only parameters that can be adjusted is the mean turbulence altitude on the HeNOS bench ($h_{0,\mathrm{H}}$). This leads to $h_{0,\mathrm{H}} = 12.9 h_{0,\mathrm{N}} = 67.0$ km.

Objective 3 can be achieved by keeping the same turbulence profile as NFIRAOS but stretching it by a factor $f_s = 12.9$. Objective 2 can then be satisfied by simply increasing the distance between DM0 and DM1 by the same factor. However, because the diameter of the meta-pupil on DM1 (ensemble of the footprint of all NGSs within the FOV—each NGS has a 13.5-mm footprint) is larger than DM1 clear aperture, which is 24.5 mm, $f_s = 12.9$ does not work well. The maximum meta-pupil diameter at the conjugate altitude of DM1 is

Table 1 NFIRAOS parameters.

Abbrv	Name	Unit	NFIRAOS
D_{N}	Telescope diameter	m	30
d_{N}	DM actuator pitch	m	0.5
λ_{N}	Imaging wavelength	μm	1.6
$h_{\mathrm{DM,N}}$	DM altitudes	km	[0, 11.2]
$r_0(0.5\ \mu\mathrm{m})$	Fried parameter	m	0.186
h_{N}	Turbulence layer altitudes	km	[0, 0.5, 1, 2, 4, 8, 16]
w_{N}	Turbulence layer weights		[0.4557, 0.1295, 0.0442, 0.0506, 0.1167, 0.0926, 0.1107]
$r_{0,\mathrm{N}}(\lambda_{\mathrm{N}})$	Fried parameter at observing wavelength	m	0.75
$\theta_{0,\mathrm{N}}(\lambda_{\mathrm{N}})$	Anisoplantic angle	arcsec	9.4
$\theta_{2,\mathrm{N}}(\lambda_{\mathrm{N}})$	Generalized anisoplantic angle after 2 DM correction	arcsec	34.6

$$D_{\mathrm{meta}} = D_{\mathrm{H}} \frac{24.5}{13.5} = 14.5\ \mathrm{m}. \tag{2}$$

It follows that the maximum conjugate altitude of DM1 is

$$h_{\mathrm{DM1,H}} = \frac{D_{\mathrm{meta}} - D_{\mathrm{H}}}{\mathrm{FOV_H}(\lambda_{\mathrm{H}})} = 123\ \mathrm{km}, \tag{3}$$

which corresponds to a maximum stretch factor of

$$f_s = h_{\mathrm{DM1,H}}/h_{\mathrm{DM1,N}} = 11. \tag{4}$$

The only way to satisfy Objectives 2 and 3 with the maximum stretch factor derived above is to reduce $r_{0,\mathrm{H}}$ to

$$r_{0,\mathrm{H}}(\lambda_{\mathrm{H}}) = 0.751\ \mathrm{m}. \tag{5}$$

This $r_{0,\mathrm{H}}$ value is still close to d_{H}, and thus Objective 1 is still achieved. It is worth noting that $r_{0,\mathrm{H}}$ actually does not depend on λ_{H}. Also interesting is that the maximum stretch factor is very close to the ratio between the NFIRAOS and the HeNOS FOVs. This coincidence was not planned. It arises from the difference in size of the two DMs. In retrospect, we realize that if the second DM had been significantly smaller, we might not have been able to scale HeNOS properly.

The fitting error is given as

$$\sigma_{\mathrm{fit,H}} = \frac{\lambda_{\mathrm{H}}}{2\pi} \sqrt{0.23 \left(\frac{d_{\mathrm{H}}}{r_{0,\mathrm{H}}(\lambda_{\mathrm{H}})} \right)^{5/3}} = 59\ \mathrm{nm\,rms}, \tag{6}$$

where $\lambda_{\mathrm{H}} = 670$ nm. The same equation gives $\sigma_{\mathrm{fit,N}} = 87.7$ nm rms for NFIRAOS. The agreement between the bench and NFIRAOS could be improved by reducing the

NFIRAOS reference wavelength. The Strehl ratio (SR) is given as

$$SR_{\mathrm{fit,H}} = \exp\left[-0.23\left(\frac{d_{\mathrm{H}}}{r_{0,\mathrm{H}}(\lambda_{\mathrm{H}})}\right)^{5/3}\right] = 0.74. \tag{7}$$

The same equation gives $SR_{\mathrm{fit,N}} = 0.89$ for NFIRAOS.

The bench parameters described above are summarized in Table 2. Note that in Ref. 2, the derived parameters were different, especially the stretch factor, which was only 4.2. This is because the need to limit the FOV to 10.9 arcsec was not recognized in Ref. 2.

In Ref. 2, we simulated NFIRAOS and HeNOS with four LGSs, and Table 5 of Ref. 2 summarizes the results. The total RMS wavefront error for HeNOS and NFIRAOS are 93 and 156 nm, leading to a delivered SR of 0.49 and 0.69, respectively, at their respective wavelength. These simulation results remain valid even if the stretch factor is different because the FOV and asterism diameter have been scaled accordingly. While HeNOS has lower wavefront error, the lower wavelength increases the sensitivity of the SR, and therefore departure from nominal performance should be easily detectable.

Table 2 HeNOS parameters.

Abbrv	Name	Unit	HeNOS
D_{H}	Telescope diameter	m	8
d_{H}	DM actuator pitch	m	0.89
λ_{H}	Imaging wavelength	μm	0.67
$h_{\mathrm{DM,H}}$	DM altitudes	km	[0, 123]
f_s	Scaling factor		11
$r_{0,\mathrm{H}}(\lambda_{\mathrm{H}})$	Fried parameter at observing wavelength after applying f_s	m	0.751
$\theta_{0,\mathrm{H}}(\lambda_{\mathrm{H}})$	Anisoplantic angle	arcsec	0.854

3 Bench Components and Calibration

The bench is built based on the bench parameters described in Sec. 2 and Table 2. Figure 1 shows its most updated optical paths, and Table 3 summarizes the abbreviated components. In order to understand the experimental results on the HeNOS bench and use them for NFIRAOS and other AO developments, it is important to know the precise dimensions of the bench. The actual as-built parameters may deviate from the design parameters but only to a small degree. In this section, we describe each component of the HeNOS bench in detail and report the calibration results. The earlier bench development and calibration results can be found in Refs. 3 and 4. NFIRAOS will be operated at −30°C, and its components will be tested under the low temperature; however, the HeNOS bench is designed to work at only room temperature, and we do not discuss the cold environment here.

3.1 *Laser Guide Star*

To measure the bench's as-built parameters, we fix one parameter and derive all others. We chose the LGS asterism size as the fixed parameter since the LGSs are mounted in solid holes on a metallic plate, which are sturdy and least likely to change over time.

NFIRAOS will project its six LGSs within a radius of 35 arcsec on sky (one at the center and five on the circle), whose stretched correspondence on HeNOS is 6.4 arcsec. For simplicity, we designed the HeNOS bench with four fixed LGSs with a square asterism. For a square asterism, the corresponding side length is 4.5 arcsec. In order to preserve the LGS cone angle through the turbulence (and therefore keep a realistic focal anisoplanatism), we also multiply the nominal range of the LGS by the stretch factor ($90\ \mathrm{km} \times 11 = 990\ \mathrm{km}$). This value provides a reasonable overlap even at the highest turbulence layer, now at $16\ \mathrm{km} \times 11 = 176\ \mathrm{km}$. The LGS footprint at this layer is $8\ \mathrm{m} \times (990 - 176)/990 = 6.6\ \mathrm{m}$, and the footprint of two LGSs, 4.5 arcsec apart, are separated by 3.8 m, leaving 1.8 m or about 30% overlap.

All four LGSs are made with single-mode fiber laser diodes from Thorlabs (LPS-675-FC), whose optical output power is 2.5 mW. The laser diodes are controlled by a combination of an ADLINK data acquisition card (DAQe-2502) and a custom printed circuit board manufactured by Alberta Printed Circuit

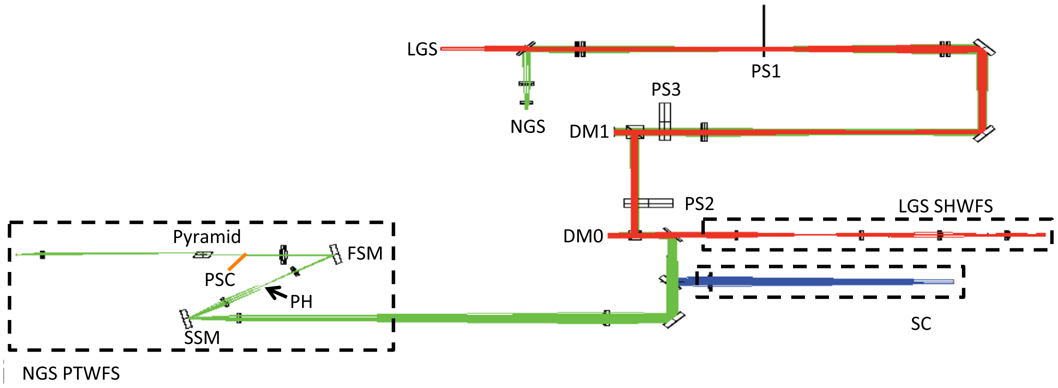

Fig. 1 The optical paths of the HeNOS bench. Abbreviations are described in Table 3. The bench consists of four LGSs in a 2×2 configuration, a grid of NGSs, two DMs conjugated to 0 and 12 km, three PSs conjugated to 0.6, 5.2, and 16.3 km, one SHWFS (red) simultaneously measuring four LGSs, one SC (blue), and one TWFS made with a double pyramid (green). To calibrate the PWFS performance, one more science camera focused on NGS, called PSC (orange), is also added.

Table 3 Bench components.

Abbrv	Name	Description
LGS	Laser guide star	2 × 2 configuration lasers whose separation defines 4.5 arcsec on the sky.
NGS	Natural guide star	Creates a grid of NGSs, previously by MA, future by pinhole mask.
DM0	Deformable mirror 0	ALPAO DM with 97 actuators at ground (0 km).
DM1	Deformable mirror 1	ALPAO DM with 277 actuators at high altitude (12 km).
PS1	Phase screen 1	UCSC (paint spraying) PS at ground layer (0.6 km).
PS2	Phase screen 2	Lexitex (index matching) PS at middle layer (5.2 km).
PS3	Phase screen 3	Lexitex (index matching) PS at high layer (16.3 km).
FSM	Fast steering mirror	Newport FSM-300.
PH	Pinhole	500 μm pinhole at NGS focus to block all but one NGS.
SSM	Star selection mirror	Zaber motorized gimbal mount and mirror.
SHWFS	Shack–Hartmann WFS	30 by 30 subapeture SHWFS with PointGrey Grasshopper (2448 × 2048, 3.45 μm pixel).
SC	Science camera	Andor sCMOS Zyla (2048 × 2048, 6.5 μm pixel) currently at LGS focus.
PTWFS	Pyramid truth WFS	76 pixel diameter pupil PWFS with PointGrey Flea (638 × 488, 5.6 μm pixel).
PSC	Pyramid science camera	PointGrey Grasshopper (2448 × 2048, 3.45 μm pixel) at NGS focus.

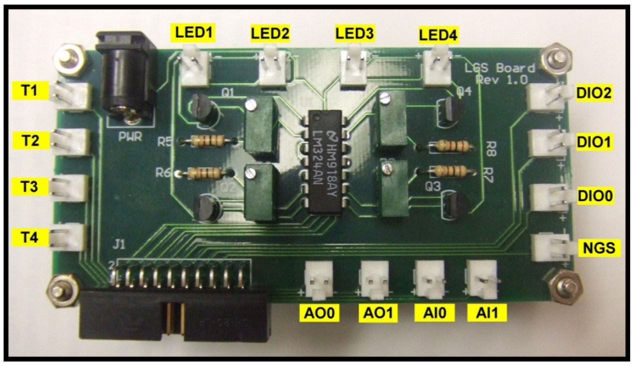

Fig. 2 A photo of the LGS board. It provides an interface for the four LGSs, NGS, and SHWFS camera trigger.

(Fig. 2). Using the DAQ card, the LGS timing and intensity can be controlled using computer commands.

3.2 *Natural Guide Star*

To evaluate the AO performance across the entire science field, many PSFs on the science camera are needed. We originally created a grid of NGSs using a laser diode (same one as LGSs) and a microlens array (MA). The use of an MA was an easy way to produce many PSFs at the focus, but it creates a grid intensity pattern on the pupil [Fig. 3(a)]. This grid pattern is likely created by the concentrated light from the gaps between microlenses on top of the pupil.

We are currently working on a new NGS design without an MA. The new design consists of a powerful LED, a collimating lens, a diffuser, and a pinhole mask in a lens tube. Figure 3(b) shows the test setup. To produce a PSF, the size of the pinhole has to be smaller than the diffraction limit of the bench, which is ∼10 μm at the NGS position in Fig. 1. The HeNOS bench uses many beamsplitters, including two beamsplitter cubes in front of the DMs, which waste a large fraction of photons, and the tiny pinhole blocks even more photons unlike the MA. We are adjusting the position of the collimating lens and pinhole mask to maximize photon count at the pinhole mask and adjusting the beamsplitters using different reflection-transmission ratios to give more weight to the NGS path.

For a temporary solution, we are using the laser diode itself, without MA nor pinhole mask, as a single NGS. The size of the laser diode is small enough to create a diffraction-limited PSF. Because it is only one PSF, we cannot evaluate AO performance over a whole FOV on the science camera, but it is used for a PTWFS experiment (see Secs. 3.9 and 4 for more about PTWFS). For performance evaluation, we place the science camera at the LGS focus and use LGSs as PSFs (see Sec. 3.6).

We are also looking into a design where the pinhole mask can be easily replaced by a single pinhole of a large radius. Using a bigger pinhole, we can experiment a wavefront sensing on an extended object using PWFS. This experiment is not a direct simulation of NFIRAOS; however, it is useful to advance observations. See Ref. 5 for PWFS simulations with extended guide objects and their science applications. Using a larger pinhole, the NGS is no longer diffraction-limited, and thus we cannot evaluate the performance directly from PSF. But since we have a separate LGS-SHWFS, we can check its performance using SHWFS measurements.

3.3 *Deformable Mirror*

We use two magnetic DMs from ALPAO, whose specifications are listed in Table 4. Since both DMs have the same actuator pitch, they are located in the same collimated space, with

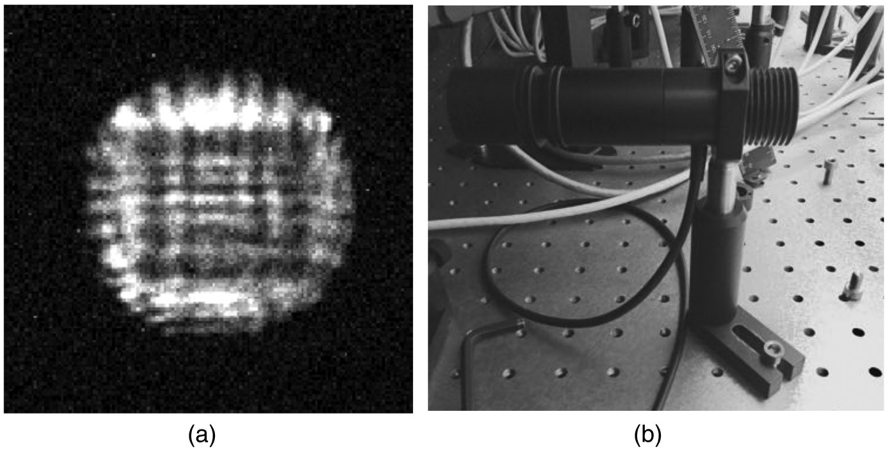
(a) (b)

Fig. 3 (a) Image of a grid pattern pupil from the old NGS light source with an MA. The grid pattern is likely created by the concentrated light from the gaps between microlenses on top of the pupil. (b) New NGS light source test setup on the bench. The new design uses a pinhole mask instead of an MA.

Table 4 DM specifications.

Name	DM0	DM1
Model	Hi-Speed DM97-15	Hi-Speed DM227-15
Actuator	97 (11 × 11 square)	277 (19 × 19)
Actuator pitch	1.5 mm	1.5 mm
Pupil diameter	13.5 mm (9 pitches)	24.5 mm (16.3 pitches)
Bandwidth	>750 Hz	>800 Hz
Settling time (±5%)	1.0 ms	1.0 ms

DM1 conjugated to the high altitude and DM0 to the ground (see Fig. 1 for their locations). Beamsplitter cubes are placed in front of both DMs so that the incident beam hits the DM surfaces normally. These cubes simplify the bench design but waste a significant fraction of photons (see Sec. 3.2 for their drawback).

We determine the actuator spacing and the altitude conjugation of the mirrors by looking at the poke matrix taken with an SHWFS (see Sec. 3.5 for SHWFS details). From the poke matrix, we measure the actuator positions in the WFS geometry and fit a uniform grid to them using a least square fit. The center of the fit is used to better align the SHWFS to avoid vignetting of the pupil. The actuator spacing derived from the scaling of the fit to DM0 is 0.914 m, and the conjugation altitude of DM1 estimated from the shear of the metapupils, knowing the LGS separation is 4.5 arcsec, is 121 km with the stretch factor, f_s, applied (12 km without).

3.4 *Phase Screen*

A key requirement of the HeNOS bench is the ability to generate realistic turbulence. To achieve this, we adopt well-calibrated turbulence screens: two screens from Lexitek[6] and one from UCSC.[7] Lexitek screens use an index matching technique, where the turbulence profile can be flexibly designed with any r_0 but is expensive. The UCSC screen uses the acrylic paint spraying technique, where the cost is less, but only small r_0 is available.

The two Lexitek phase screens (PS2 and PS3 in Fig. 1) are placed in the same collimated space as the two DMs. PS3 just before DM1 has the bigger r_0 and simulates the highest turbulence layer, and PS2 in between the two DMs simulates the middle layer turbulence. Because the UCSC screen (PS1) is conjugated to the ground, which is occupied by DM0, a separate pupil position is created (see PS1 position in Fig. 1). At this position, the designed beam size is 10 mm.

Two Lexitek PSs are mounted on Lexitek motorized rotary stages (LS-100), and the UCSC PS is controlled by a Galil motion controller. To measure wind speed, we measure the distance between the optical axis and the rotation center. The relationship between the physical dimensions and the simulated ones is given by the simulated telescope size and the physical pupil size in the collimated space (see Sec. 3.7 for the simulated telescope size). From this relationship, the circumferences of three PSs are 295 (PS1), 97 (PS2), and 92 m (PS3). Note that due to the rotational movement, the speed is never uniform across the metapupil.

The altitudes of the PSs are calculated from the physical positions of the optical surfaces. Knowing the physical position (actual physical distance between DM0 and DM1 on the bench measured by a ruler) and the simulated altitude (Sec. 3.3) of DM1, the scaling factor relating the bench and the altitude of the atmosphere in the collimated space, where DM0, DM1, PS2, and PS3 are placed, is 28.22 mm/km. The scaling factor is proportional to the square of the aperture size ratio, and thus the PS1 altitude is $28.22 * (10/13.5)^2 = 15.8$ mm/km, where aperture sizes are 10 m at PS1 and 13.35 mm at the DM0's position.

For turbulence power measurements, we derive the Fried parameter using two independent methods: (1) the full-width-half-maximum of PSFs on the SC, assuming Kolomogorov statistics ($r_{0,\mathrm{SC}}$ on Table 5), and (2) the standard deviation of the wavefront reconstructed from WFS slopes using a CuReD[8] reconstructor ($r_{0,\mathrm{WFS}}$ on Table 5). For method one, we use the NGS light source with an MA to create many stars for better statistics and take long exposure PSF images on the SC. For method two, we take the slope measurements on the SHWFS. In both cases, we use one PS and take data on 100

Table 5 Fried parameter.

Phase screen	$r_{0,\mathrm{SC}}$ (670 nm) m	$r_{0,\mathrm{SC}}$ (500 nm) m	$r_{0,\mathrm{WFS}}$ (670 nm) m	$r_{0,\mathrm{WFS}}$ (500 nm) m	r_0 (500 nm) m
PS1	0.99	0.70	1.15	0.81	0.74
PS2	2.37	1.67	2.83	1.99	1.61
PS3	3.72	2.62	3.80	2.68	2.79
All	0.83	0.58	…	…	…

different positions across the PS at a time. Data without PSs are also taken for reference. The resultant Fried parameters are listed in Table 5 along with the nominal value used by the manufacturer (r_0). Note that the measurements of the high altitude PS need to be corrected for the cone effect. All PS measurements are well within 10% of the nominal value, but $r_{0,\mathrm{WFS}}$ is larger than $r_{0,\mathrm{SC}}$. This is because the WFS is blind to the highest spatial frequencies of the turbulence, and thus we believe $r_{0,\mathrm{SC}}$ is more accurate. The relative powers of the PSs in terms of $\sigma^2 \propto r_0^{-5/3}$ are 74.3%, 17.4%, and 8.2%.

3.5 *Shack–Hartmann Wavefront Sensor*

Our WFS is a custom-made SHWFS with a square MA (300 μm pitch) and a PointGrey Grasshopper CCD (2448×2048 array with $3.45\ \mu\mathrm{m} \times 3.45\ \mu\mathrm{m}$ pixel). The FOV of the lenslets is large enough to separately see all four LGSs, and thus a single detector is used to sense all four LGSs simultaneously. Depending on the experiment, individual LGS can be used as well if separate measurements are required. Our SHWFS has many subapertures (30 across the pupil) to sample the elongation finely at each distance away from the center.

We identify the spots created by the MA, and the average separation of the LGSs is 20.58 ± 0.51 pixel, which translates to the WFS pixel size being 0.22 arcsec. We fit a uniform grid to the SHWFS spots and define subapertures, including the ones outside of the illuminated zone. We then determine the pupil size by matching the measured illumination pattern and a modeled illumination pattern. The modeled illumination is the percentage coverage map of subapertures when a perfect circle is projected on a square subapertures. Applying this method to four LGSs separately, we find the radius of the pupil on the SHWFS to be 15.226 subapertures.

Assuming a small aberration approximation, we estimate a WFS fitting error using SR (SR) of NGS. First, we measure SR_1 using flat mirrors instead of DMs and no phase screens. Then, we measure SR_2 using DM0 and a ground layer PS after closing loop. The error is estimated as

$$\sigma_{\mathrm{AO}}^2 = \ln \frac{\mathrm{SR}_1}{\mathrm{SR}_2}. \tag{8}$$

Using median SRs, $\sigma_{\mathrm{AO}} = 33$ nm.

More thorough derivation of the error budget can be found in Ref. 9.

3.6 *Science Camera*

We originally used a PointGrey Grasshopper (2448×2048, 3.45 μm pixel), the same model as the one used in the SHWFS, for the science camera; however, we realized that the Grasshopper has two readout channels that create background offset between the two sides of the detector. When a PSF falls near this divided region, it adds spatially different noise properties and complicates the modeling. We also noticed that the offset varies from time to time. We thus replaced the camera with an Andor sCMOS Zyla (2048×2048, 6.5 μm pixel), which has a low noise and almost uniform background. The Andor sCMOS has a similar number of pixels but with larger pixels, and we realigned the lenses in front of it to have the same plate scale as when a Grasshopper was used.

Due to the NGS light source problem (Sec. 3.2), currently we do not have a proper NGS light source on the bench. While we work on new solutions, for a temporary fix, we locate the science camera at the focus of the LGSs and use them as science targets. At this location, their plate scale is 5.6 milli-arcsec.

3.7 *Telescope Size*

The simulated on-sky telescope diameter was measured in the earlier stages of bench development using the PSF Airy rings. The bench had flat mirrors instead of DMs, an NGS light source with an MA, no PSs, and an iris at PS1's position. We used a 3-mm iris to have the first ring distant enough from the core while keeping a sufficiently bright aperture to measure its size.

We took an image on the science camera and identified PSFs on the image. To obtain a high SNR, we stack all PSFs by aligning the brightest pixels [Fig. 4(a), the core masked out]. To measure the diameter of the ring, we linearized the PSF image by transforming it from polar to Cartesian coordinates [Fig. 4(b)]. The radius of the ring is the median position of the central line and is $1.64\,\lambda/D$, which corresponds to an aperture of 2.44 m on sky. Scaling it to the 10-mm aperture at the first pupil's position (PS1's position), the HeNOS telescope size is 8.13 m.

3.8 *SHWFS Spot Elongation and Truth Wavefront Sensor*

When a sodium (Na) laser is used as an LGS, the spots on an SHWFS are radially elongated due to the finite thickness of the Na layer. When the Na layer profile (i.e., height, thickness, and density distribution) changes, the photon distributions in the elongated spots also change. This introduces an additional centroid shift when centroding is applied.[10] This spot elongation problem is more severe as the diameter of a telescope increases. Figure 5 explains how the thickness of the Na layer produces more elongated spots with larger telescopes, and why the fluctuation in Na profile causes aberrations. See for example Ref. 11 for more detail about SHWFS elongation and imperfection in centroiding.

To simulate the SHWFS elongation created by the Na layer, we apply a set of defocus commands to DM0 and change the LGS intensity according to the empirically obtained Na profile while the LGS-WFS camera shutter is open (or take individual WFS image and combine all). An example of the empirical Na profiles taken by the University of British Colombia group is shown in Fig. 6, and its reproduced SHWFS elongation at $t = 0$ s is shown in Fig. 7.

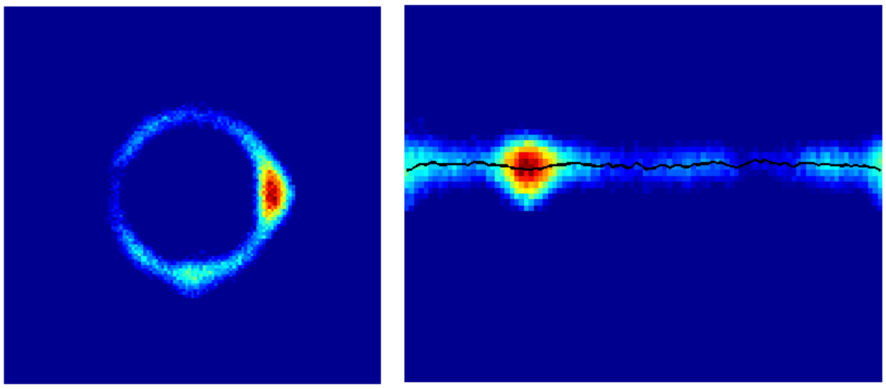

(a) (b)

Fig. 4 To measure the simulated telescope size, many PSFs on the SC created by NGS source with an MA are stacked. (a) The core-masked stacked PSF. (b) The stacked PSF is then linearized by transforming from polar to Cartesian coordinate, and the radius of the ring is the median position of the central line.

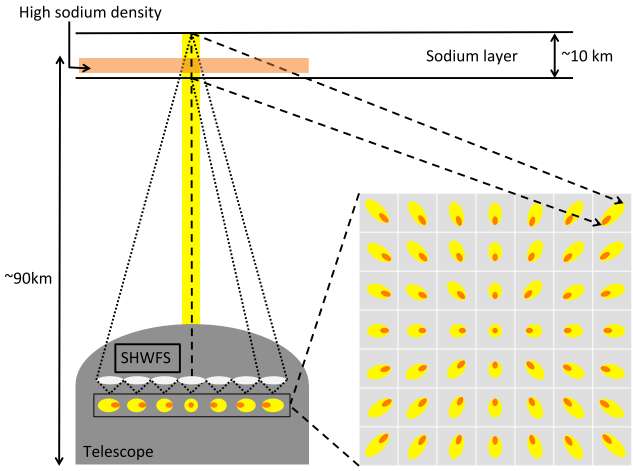

Fig. 5 Schematic of LGS SHWFS spot elongation. The example spots shown here are for a center-launched LGS. The subapertures further away from the center see the Na layer with an angle compared to those near the center, resulting in more radially elongated spots. This offset from the center increases with telescope size, and is particularly severe for ELTs. The layer shown as orange in the sodium layer represents high Na density, and its location in SHWFS spots are also shown as orange. Because of the high Na density, the orange part of the spots has higher flux return, which would be confused as a radial spot shift.

3.9 *Pyramid Truth Wavefront Sensor*

The one major update to HeNOS is the implementation of a TWFS made with a PWFS. This is to follow up on the NFIRAOS' new decision to use a PWFS instead of an SHWFS for its TWFS (Ref. 12). The description of general TWFS functions and the HeNOS TWFS design are reported in Ref. 11, and our optical design is shown in Fig. 1 in green. In short, on HeNOS, the grid of NGSs hitting a star selection mirror (SSM) at the pupil is sent to a pinhole where only one NGS goes through. The single NGS beam is then modulated by a fast steering mirror (FSM) at the pupil, and the focused beam makes a circle around the vertex of the pyramid. The light is distributed in four directions and a relay lens behind the pyramid forms four separate pupil images on a detector. The incoming wavefront can be measured by comparing their intensity patterns.

Our SSM and FSM use a Zaber Motorized Gimbal Mount and a Newport FSM-300, respectively. While the Zaber controller is run by USB, the FSM-300 controller requires analog inputs, and thus we installed the same ADLINK data acquisition card (DAQe-2502) as the laser diodes in the HeNOS computer. The interface between the DAQ card and the FSM controller is an off-the-shelf ADLINK terminal board. The PWFS camera is a PointGrey Flea (648×488 array with 5.6 μm pixel). To

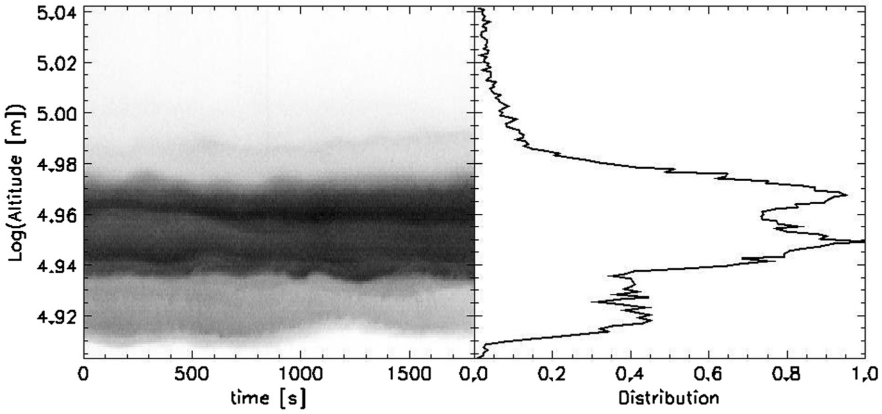

(a) (b)

Fig. 6 (a) Empirically obtained Na profiles as functions of time over 1800 s. Darker color for higher density. (b) one-dimensional plot of Na profile at $t = 0$ s.

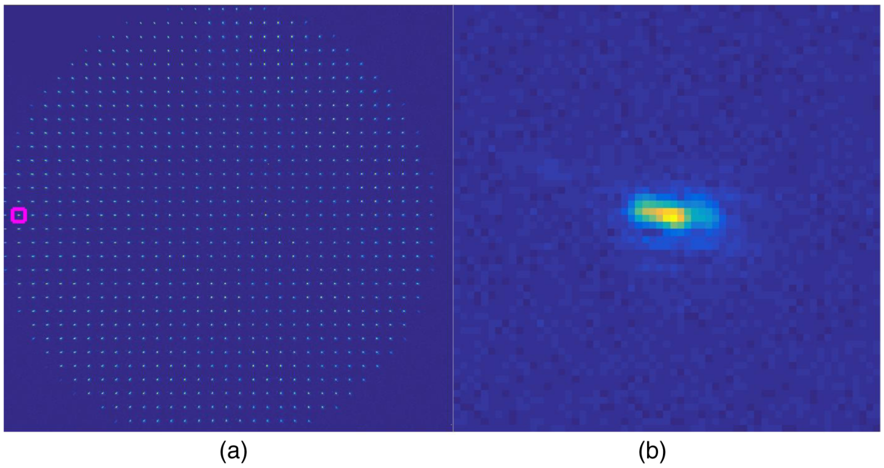

Fig. 7 Simulated elongated SHWFS spots when Na profile at $t = 0$ [Fig. 6(b)] is applied. (a) Full frame SHWFS camera image and (b) one zoomed spot in a magenta box.

Table 6 As-built HeNOS parameters.

Parameter	Unit	Design	Measurement
LGS asterism	arcsec	4.5	4.5
Telescope size	m	8	8.13
Actuator distance	m	0.89	0.914
Subaperture size	m	0.27	0.267
Science FOV	arcsec	10.9	11.04
DM altitude	km	[0, 11.2]	[0, 12]
r_0(500 nm)	m	0.609	0.584
Phase screen altitude	km	[0, 4.2, 14]	[0.6, 5.2, 16.3]
Phase screen strength	%	[72.3, 19.8, 7.9]	[74.3, 17.4, 8.2]
LGS altitude	km	90	98.5

Table 7 Desired versus obtained objective.

Objective	Metric	Desired	Obtained	Error
1	r_0/d_H	1.0	0.92	8%
3	FOV$/\theta_0$	12.8	9.8	23%
2	FOV$/\theta_2$	3.5	2.9	17%
2 and 3	θ_2/θ_0	3.7	3.4	8%

evaluate the PSF at the tip of the pyramid, we have inserted one more beamsplitter between the focusing lens and the pyramid and added one more camera (pyramid science camera, PSC, orange path in Fig. 1). The PSC is a PointGrey Grasshopper (2448×2048, 3.45 μm pixel). Both the PWFS camera and the PSC are also connected to the ADLINK terminal board so that the PWFS camera, PSC, and FSM are all synchronized.

Our pyramid component is a double pyramid borrowed from the Arcetri group. A double pyramid consists of two pyramid-shaped prisms glued back to back. The two prisms are made with different materials (i.e., different index of refraction) to compensate for chromatic aberrations. Alternative pyramid components, such as double roof prisms, can be used (see, e.g., Ref. 11 for performance comparisons between different pyramid components).

3.10 *Bench Summary*

All calibration results described in this section are summarized in Table 6. For simplicity, the values here are not including the stretch factor, f_s, described in Sec. 2. Table 7 summarizes how the as-built bench matches the design objective from Sec. 2. In general, the parameters of the HeNOS bench are in reasonable agreement with the desired parameters. In any case, the most important is to know the as-built parameters so that the models can be parameterized correctly. Knowing the HeNOS parameter well, we are ready to demonstrate and test the techniques that will be used on NFIRAOS and other instruments/AO systems. Please refer additional HeNOS tests in Refs. 9 and 13 for an SLODAR experiment and NCPA calibration using the focal plane sharpening method.

4 Closing the Loop

Right now, we use a flat mirror at the DM1's position to simplify the calibration procedures and bench development, and thus the HeNOS bench only supports single-conjugate adaptive optics (SCAO). With the SHWFS and the newly implemented PWFS, HeNOS offers three different modes: LGSAO with an SHWFS, NGSAO with a PWFS, and LGSAO with an elongated SHWFS corrected by an NGS-PTWFS. For all modes, we simulate each frame step by step instead of running the bench in real time so that we can isolate and understand the effect of individual step/component. When we simulate each step, for example, (1) turn on LGS laser and (2) take SHWFS image in Fig. 8, we include extra waiting time in each step to make sure the laser is fully lased and the SHWFS image is completely transferred to computer. Because of these waiting times, simulating frames take a long time. Study of hardware latency, such as DM and WFS latency, and optimization of real-time controller will be a separate experiment in the future.

4.1 *LGSAO with SHWFS*

The steps to simulate the classical SCAO with LGS and SHWFS are shown in Fig. 8. The numbers in the flowchart indicate the order of process called in the loop. Currently, it takes about 3 s to take one frame on the bench, which leads to several hours of run-time for any experiment. We noticed that, over this time, the SR of the long exposure image drops while the instantaneous Strehl stays stable. This is indicative of a TT error at the WFS. The cause of this TT error is probably produced by the flexure in the paths. In the WFS and science paths on HeNOS after DM0, optical components, including WFS camera, are mounted in between four rods (called cage system) that are keener to thermal expansion. To correct this, we neglect the TT from the LGSWFS and use the TT from the SC (steps 9 and 10 in Fig. 8). This method prevents TT errors at the SC: the long exposure SR no longer drops and remains comparable to the average short exposure SR.

This mode is the most developed and most used mode on the HeNOS bench. Using this mode, we collaborate with TMT

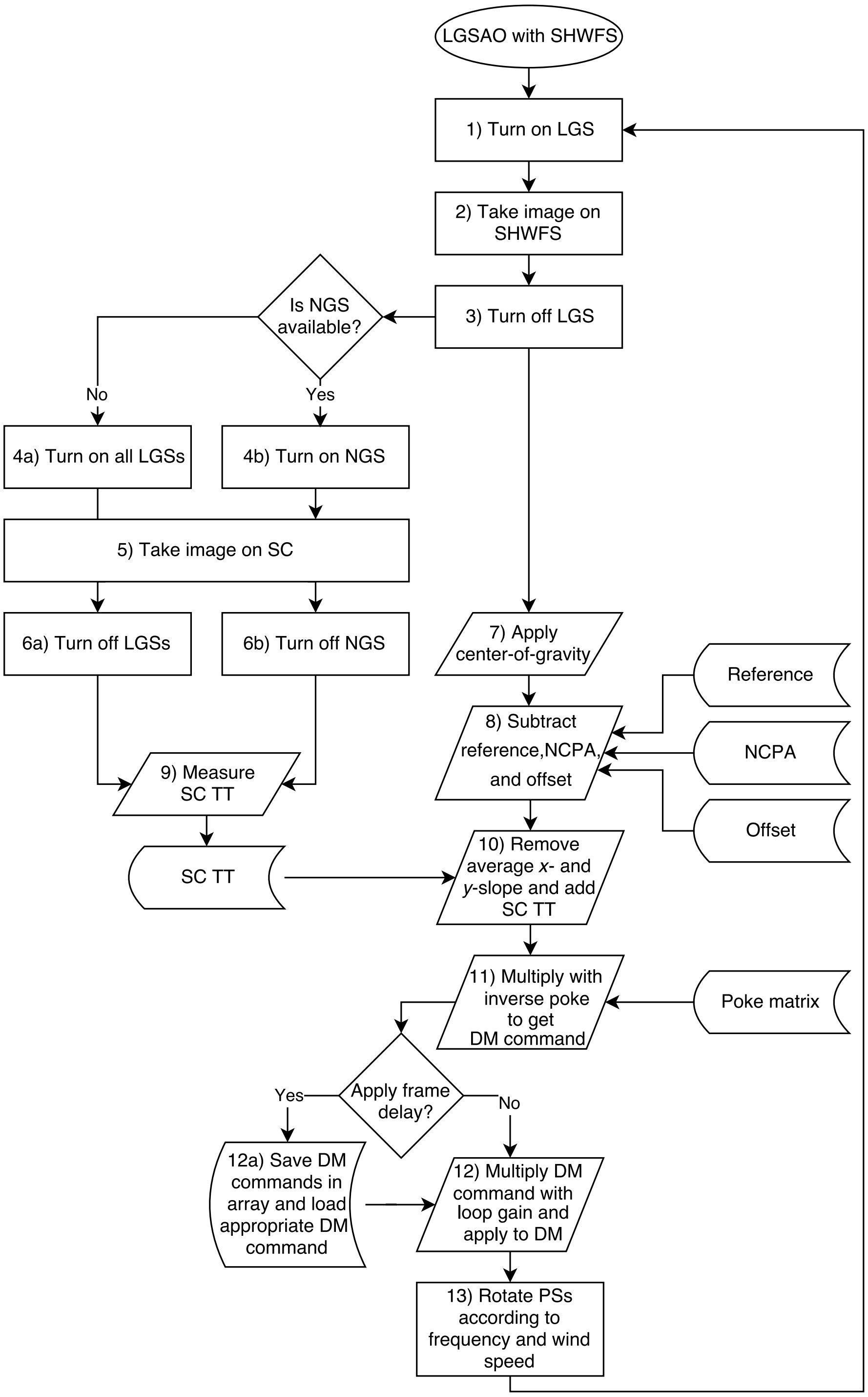

Fig. 8 Flowchart describing how the SCAO loop is closed using the LGS and the SHWFS on HeNOS. The numbers indicate the order of process called in the loop.

Observatory Corporation and Laboratoire d'Astrophysique de Marseille to demonstrate PSF reconstruction techniques by comparing the empirical data with analytic models (Refs. 14 and 15).

4.2 *NGSAO with PWFS*

With the implementation of the PWFS, the bench now can be closed with the NGS and the PWFS. The steps of this mode are shown in Fig. 9.

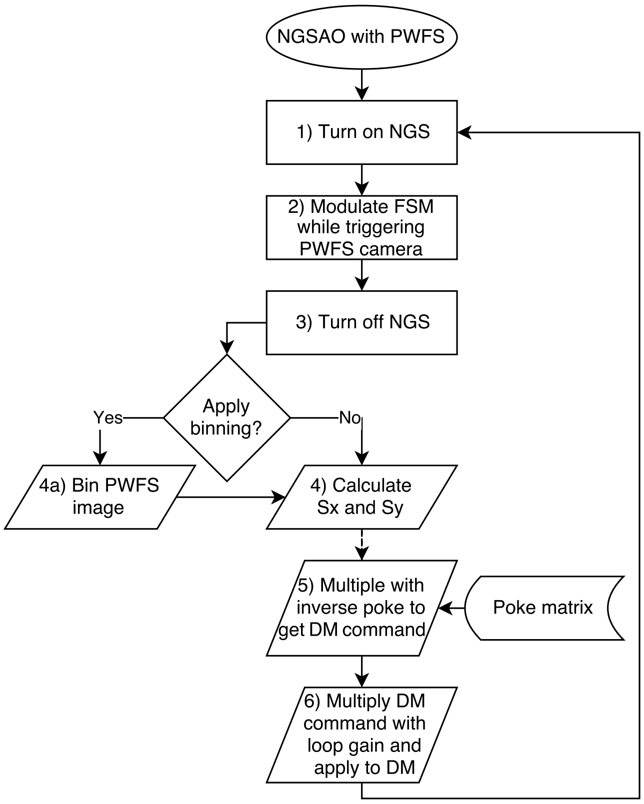

Fig. 9 Flowchart describing how the HeNOS bench closes the loop with NGS and PWFS. The numbers indicate the order of process called in the loop.

As an example, (A) PSF, (B) raw PWFS image, (C) *x*- and (F) *y*-slope signal, (D) DM0 shape, and (E) reconstructed wavefront before [Fig. 10(a), zero commands on DM0] and after [Fig. 10(b)] the loop is closed are shown. In this example, there are no PSs in the path. The initial PSF is big and fuzzy, and after closing the loop, the diffraction rings are visible.

Because the main purpose of the PWFS is a TWFS, this NGSAO with PWFS mode is currently quite basic. Once the new NGS source with a larger pinhole is added (Sec. 3.2), we will experiment wavefront sensing on an extended object with PWFS. Extended wavefront sensing in general is useful to increase the sky coverage, but also its application includes the use of LGS on a PWFS. As PWFS becomes a more popular choice for many future upgrades (e.g., GPI, Subaru, and Keck), the PWFS mode on the HeNOS bench is an interesting capability for future experiments.

4.3 *LGSAO with Elongated SHWFS and NGS PTWFS*

The last mode available on the HeNOS bench is the loop with the LGS-SHWFS using the elongated SHWFS spots and the NGS-TWFS correction. The flowchart in Fig. 11 shows the steps.

Because of the alignment imperfection in the PWFS path, as the amount of defocus applied on DM0 changes, the position of the beam at the tip of the pyramid drifts. To fix this problem, we update the zero-position of FSM each time (PWFS centering at the step 13). The new zero-position is measured by comparing the vertical and horizontal pupil intensities. As we apply the evolving Na profile (Fig. 6), the mean height of Na layer (thus focus term) needs to be measured. In the TMT +NFIRAOS case, the TWFS does not measure the defocus term and only measures higher order radial modes, but on the HeNOS bench, we measure the defocus term using the TWFS as well because we do not have a separate focus WFS.

Figure 12 shows one example of closing loop with the elongated SHWFS. Starting with the best DM flat from the previous day, the loop is closed using the elongated SHWFS spots. For this experiment, we apply the same Na profile shown in Fig. 6(b) for all iterations (i.e., Na profile does not evolve). We use a higher loop gain of 0.5 for this test to speed up the simulation. Before the TWFS feedback is applied [Fig. 12(a)], DM changes

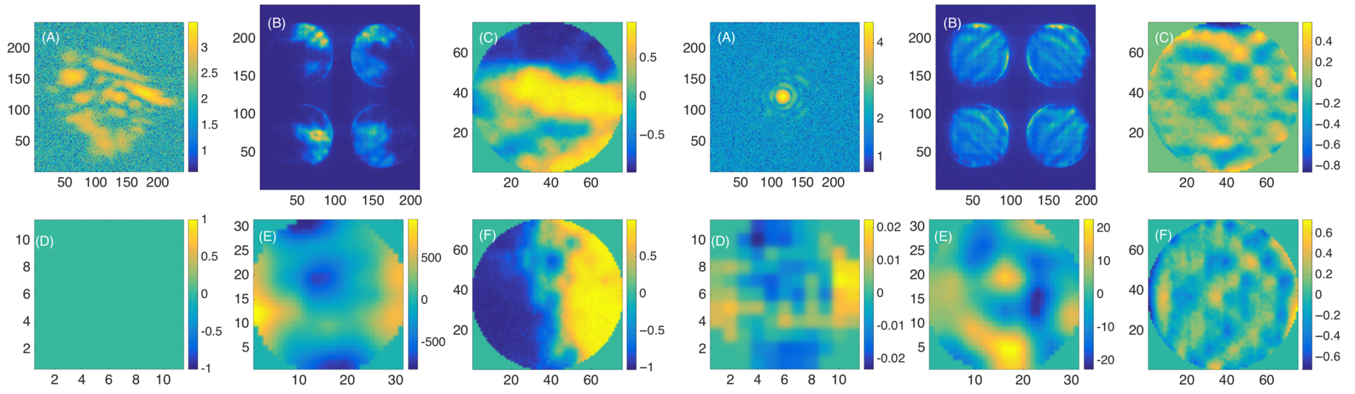

(a)

(b)

Fig. 10 (A) PSF on PSC, (B) raw pupil image, (C) *x*- and (F) *y*-slope signal, (D) DM0 shape, and (E) reconstructed wavefront. (a) Starting from zero command, (b) the loop is closed after 50 iterations with loop gain = 0.2, and diffraction rings are seen in the PSF (panel A).

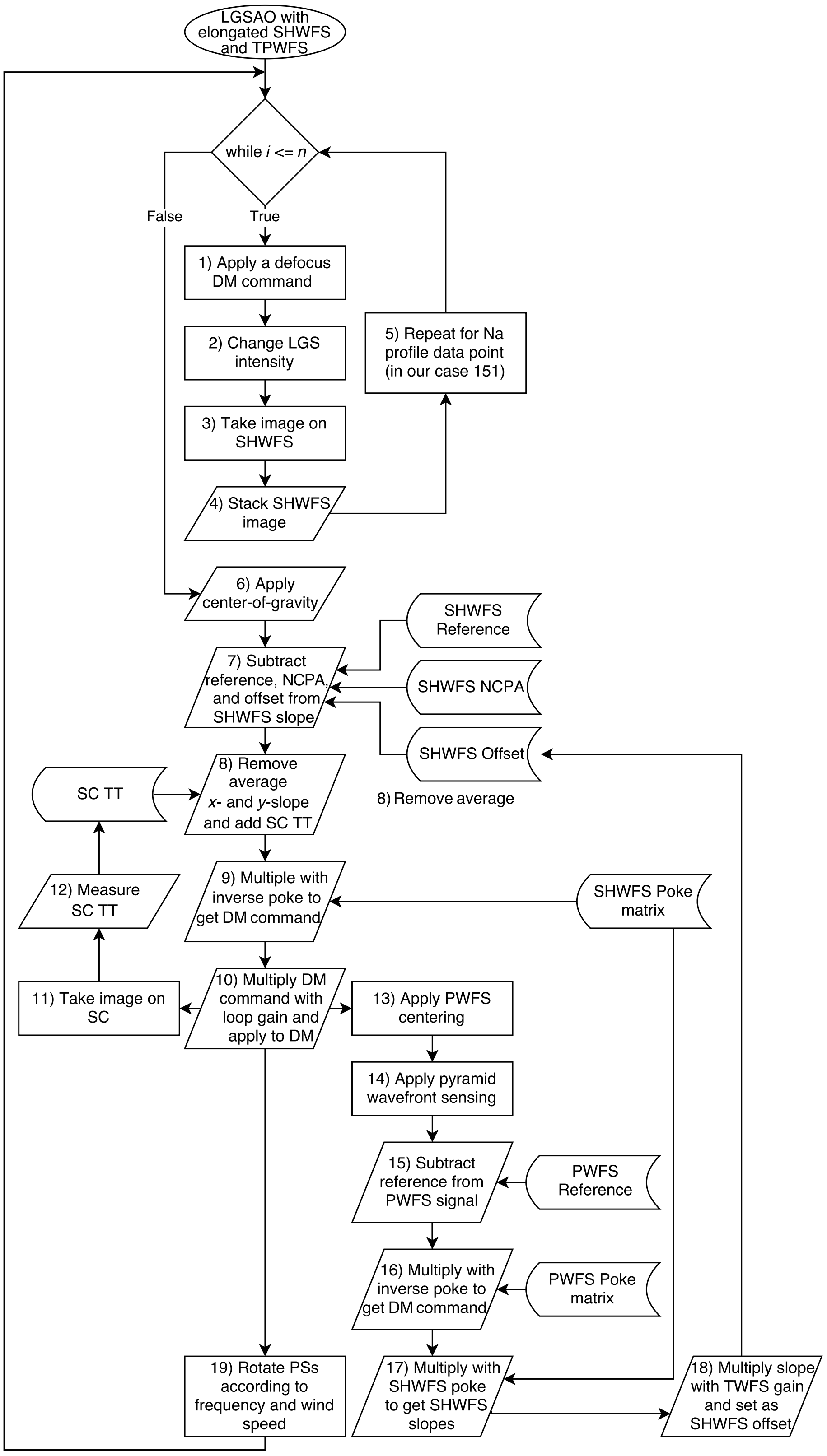

Fig. 11 Flowchart describing how the elongated SHWFS is integrated into the SCAO loop and how measurements from the PTWFS are fed to the loop as SHWFS offsets. The numbers indicate the order of process called in the loop.

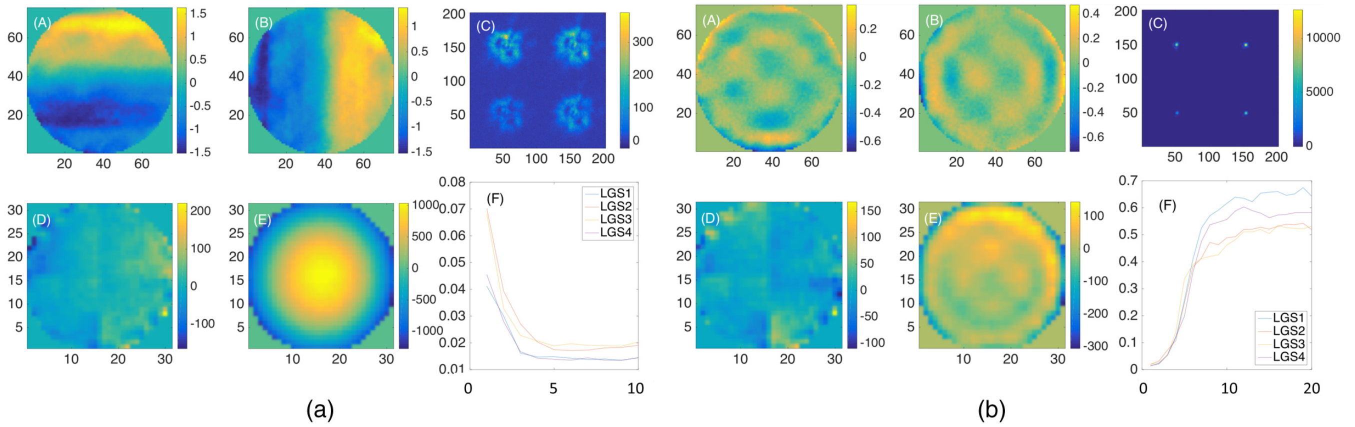

Fig. 12 (A) PWFS slope signal in x, (B) PWFS slope signal in y, (C) four LGSs on the science camera, (D) reconstructed phase using elongated SHWFS, (E) reconstructed phase using normal SHWFS, and (F) evolution of four LGS SRs while closing loop. (a) After closing loop on the elongated SHWFS spots with the Na profile shown in Fig. 6(b) without TWFS feedback. (b) After closing loop with TWFS feedback.

its shape to compensate the aberrations created in the elongated SHWFS spots by the Na profile, as described in Sec. 3.8, and thus the reconstructed phase by the elongated SHWFS (panel D) sees flat phase. However, the true wavefront on the science targets is not affected by the Na profile (the actual phase shown on panel E includes a big defocus and radial aberrations), and it actually adds “wrong” aberration onto the science targets. As a result, four LGS SRs (panel F) become low, and the final PSFs on panel C are big and fuzzy. After the loop is closed on the elongated SHWFS with Na profile, we then close the loop again but now with TWFS feedback [Fig. 12(b)]. The TWFS feedback is applied as a reference slope to the elongated SHWFS. After 20 iterations, the four LGS SRs (panel F) are improved (>50%), and all three WFSs, PWFS (panels A and B), elongated SHWFS (panel D), and normal SHWFS (panel E) see small aberrations.

5 Summary and Future Plan

We have shown the derivations of the HeNOS parameters (Sec. 2) and reported the implementation of these parameters on an optical bench (Sec. 3). The most recent upgrade is the addition of the TWFS made with a PWFS (Sec. 3.9). The truth wavefront sensing includes the simulation of the SHWFS spot elongation due to the Na layer (Sec. 3.8), and PWFS feedback as a reference slope to the SHWFS. With the new implementation of the PWFS, the HeNOS bench currently offers three different AO modes: LGSAO with an SHWFS (Sec. 4.1), NGSAO with a PWFS (Sec. 4.2), and LGSAO with an elongated SHWFS corrected by an NGS-PTWFS (Sec. 4.3). Some examples of the actual experiment performed on HeNOS can be found in Refs. 14 and 15, where we use HeNOS to demonstrate NGAO PSF reconstruction algorithm for TMT-NFIRAOS and a generalized off-axis PSF reconstruction model for extremely large telescopes, respectively.

There are several hardware and software additions to be completed soon. For hardware additions, we have started to work on a new NGS source simulator design using a pinhole mask (Sec. 3.2). We will make more measurements with the prototype [Fig. 3(b)] and finalize the design. Once the new NGS light source is built, we can move the science camera back to the NGS focus position. Currently, we use a flat mirror instead of a DM at the DM1’s position to simplify the bench for calibration purposes. Most calibrations are done, and we expect to implement DM1 soon.

For the software upgrades, we are working on including a matched filter centroiding method for the LGS-WFS. It is the method NFIRAOS will use. Currently, we close the loop only with one LGS, thus it is an SCAO loop. We are collaborating with Laboratoire d’Astrophysique de Marseille on implementing a laser tomography (LT) AO functionality to HeNOS, which can be achieved without having the second DM. LTAO mode can potentially be operated on NFIRAOS, especially when one of the two DMs fails. Once we add the second DM, we can also include multiconjugate AO. With the LTAO and MCAO capabilities, PSF reconstruction for LTAO/MCAO will also be tested.

Once all upgrades are included, the bench will not only provide an experimental anchor to the model currently used to predict the NFIRAOS performance but will also demonstrate the following:

- an MCAO configuration where the matched filter for LGS-SHWFS centroiding is updated according to changes in the sodium (Na) layer profile using one TWFS
- robustness against the spatial nonuniformity of the Na layer, where each WFS sees a different Na profile
- an MCAO configuration where field-dependent noncommon path aberrations are calibrated and compensated with turbulence, LGS elongation, and Na profile evolution via WFS slope offsets, on top of off-line (no spot elongation and no turbulence) calibration
- tomographic reconstruction using a combination of high-order LGS-WFS and low-order NGS-WFS, particularly with NGSs that are faint and/or only partially sharpened by the MCAO system.
- turbulence profile estimation using techniques similar to SLODAR (Slope detection and ranging; Refs. 16 and 17) applied to the NFIRAOS LGS-WFS measurements
- wide-field PSF reconstruction in an MCAO system.

Calibration methods, algorithms, and AO techniques developed here are all valuable not only for NFIRAOS development but also for future upgrades and developments of other instruments. We will continue developing the bench to include more functionalities to simulate NFIRAOS while collaborating with others to experiment with their new techniques.

Acknowledgments

The development of the HeNOS bench has been a collective effort of many members, including short-term postdoctoral researchers and students, and we would like to acknowledge Masen Lamb at Dunlap Institute at University of Toronto, Siqi Liu at University of Toronto, Maaike van Kooten at Leiden University, Carlos Correia at Laboratoire d'Astrophysique de Marseille, and Eric A. McVeigh for their involvement. We also would like to thank Tim Hardy and Jonathan Stocks at NRC-Herzberg for their generous technical help in hardware and software.

References

1. G. Herriot et al., "NFIRAOS: first facility AO system for the Thirty Meter Telescope," *Proc. SPIE* **9148**, 914810 (2014).
2. J.-P. Véran et al., "The HIA MCAO laboratory bench," *Proc. SPIE* **8447**, 844750 (2012).
3. P. Turri et al., "An MCAO test bench for NFIRAOS," *Proc. SPIE* **9148**, 91485Y (2014).
4. M. Rosensteiner et al., "Laboratory tests on HeNOS, the MCAO test bench for NFIRAOS," in *Adaptive Optics for Extremely Large Telescopes 4—Conf. Proc.* (2015).
5. E. Mieda, J. Fung, and J.-P. Veran, "Simulating the performance of pyramid wavefront sensors on extended objects and broadband sensing," in *Adaptive Optics for Extremely Large Telescopes 5 Proc.* (2017).
6. S. V. Mantravadi, T. A. Rhoadarmer, and R. S. Glas, "Simple laboratory system for generating well-controlled atmospheric-like turbulence," *Proc. SPIE* **5553**, 290–300 (2004).
7. R. Rampy et al., "New method of fabricating phase screens for simulated atmospheric turbulence," *Proc. SPIE* **7736**, 77362Y (2010).
8. M. Rosensteiner, "Wavefront reconstruction for extremely large telescopes via CuRe with domain decomposition," *J. Opt. Soc. Am. A* **29**, 2328 (2012).
9. P. Turri, "Advancing next generation adaptive optics in astronomy: from the lab to the sky," PhD Thesis, University of Victoria (2017).
10. M. A. van Dam et al., "Quasi-static aberrations induced by laser guide stars in adaptive optics," *Opt. Express* **14**, 7535–7540 (2006).
11. E. Mieda et al., "Testing the pyramid truth wavefront sensor for NFIRAOS in the lab," *Proc. SPIE* **9909**, 99091J (2016).
12. J.-P. Veran et al., "Pyramid versus Shack-Hartmann: trade study results for the NFIRAOS NGS WFS," in *Adaptive Optics for Extremely Large Telescopes IV (AO4ELT4) Proc.*, E31 (2015).
13. M. Rosensteiner et al., "On the verification of NFIRAOS algorithms and performance on the HeNOS bench," *Proc. SPIE* **9909**, 990949 (2016).
14. L. Gilles et al., "Point spread function reconstruction simulations and tests on the HeNOS Bench," in *Adaptive Optics for Extremely Large Telescopes 5 Proc.*, (2017).
15. O. Beltramo-Martin et al., "Off-axis point spread function characterisation in laser-guide star adaptive optics systems," *Mon. Not. R. Astron. Soc.* **478**, 4642–4656 (2018).
16. R. W. Wilson, "SLODAR: measuring optical turbulence altitude with a Shack-Hartmann wavefront sensor," *Mon. Not. R. Astron. Soc.* **337**, 103–108 (2002).
17. T. Butterley, R. W. Wilson, and M. Sarazin, "Determination of the profile of atmospheric optical turbulence strength from SLODAR data," *Mon. Not. R. Astron. Soc.* **369**, 835–845 (2006).

Biographies for the authors are not available.